

Numerical study of a highly sensitive surface plasmon resonance sensor based on circular-lattice holey fiber

Jian-Fei Liao(廖健飞), Dao-Ming Lu(卢道明), Li-Jun Chen(陈丽军), and Tian-Ye Huang(黄田野)
Citation: Chin. Phys. B, 2022, 31 (**6**): 060701. DOI: 10.1088/1674-1056/ac43a5
Journal homepage: http://cpb.iphy.ac.cn; http://iopscience.iop.org/cpb

What follows is a list of articles you may be interested in

Finite element simulation of Love wave sensor for the detection of volatile organic gases

Yan Wang(王艳), Su-Peng Liang(梁苏鹏), Shu-Lin Shang(商树林),Yong-Bing Xiao(肖勇兵), and Yu-Xin Yuan(袁宇鑫)
Chin. Phys. B, 2022, 31 (**3**): 030701. DOI: 10.1088/1674-1056/ac3ec9

Cascaded dual-channel fiber SPR temperature sensor based on liquid and solid encapsulations

Yong Wei(魏勇), Lingling Li(李玲玲), Chunlan Liu(刘春兰), Jiangxi Hu(胡江西), Yudong Su(苏于东), Ping Wu(吴萍), and Xiaoling Zhao(赵晓玲)
Chin. Phys. B, 2021, 30 (**10**): 100701. DOI: 10.1088/1674-1056/ac0426

In-situ fabrication of ZnO nanoparticles sensors based on gas-sensing electrode for ppb-level H_2S detection at room temperature

Jing-Yue Xuan(宣景悦), Guo-Dong Zhao(赵国栋), Xiao-Bo Shi(史小波), Wei Geng(耿伟), Heng-Zheng Li(李恒征), Mei-Ling Sun(孙美玲), Fu-Chao Jia(贾福超), Shu-Gang Tan(谭树刚), Guang-Chao Yin(尹广超), and Bo Liu(刘波)
Chin. Phys. B, 2021, 30 (**2**): 020701. DOI: 10.1088/1674-1056/abcf46

Fiber cladding SPR bending sensor characterized by two parameters

Chunlan Liu(刘春兰), Jiangxi Hu(胡江西), Yong Wei(魏勇), Yudong Su(苏于东), Ping Wu(吴萍), Lingling Li(李玲玲), and Xiaoling Zhao(赵晓玲)
Chin. Phys. B, 2020, 29 (**12**): 120701. DOI: 10.1088/1674-1056/aba9c1

Sensitivity enhancement of WS_2-coated SPR-based optical fiber biosensor for detecting glucose concentration

Yun Cai(蔡云), Wei Li(李卫), Ye Feng(冯烨), Jian-Sheng Zhao(赵建胜), Gang Bai(白刚), Jie Xu(许杰), and Jin-Ze Li(李金泽)$
Chin. Phys. B, 2020, 29 (**11**): 110701. DOI: 10.1088/1674-1056/aba601

Numerical study of a highly sensitive surface plasmon resonance sensor based on circular-lattice holey fiber

Jian-Fei Liao(廖健飞)[1,3], Dao-Ming Lu(卢道明)[1], Li-Jun Chen(陈丽军)[1], and Tian-Ye Huang(黄田野)[2,†]

[1] *School of Mechanical and Electrical Engineering, Wuyi University, Wuyishan* 354300, *China*
[2] *School of Mechanical Engineering and Electronic Information, China University of Geosciences (Wuhan), Wuhan* 430074, *China*
[3] *College of Physics and Electronic Information, Gannan Normal University, Ganzhou* 341000, *China*

(Received 16 October 2021; revised manuscript received 13 December 2021; accepted manuscript online 16 December 2021)

A new design of surface plasmon resonance (SPR) sensor employing circular-lattice holey fiber to achieve high-sensitivity detection is proposed. The sensing performance of the proposed sensor is numerically investigated and the results indicate that our proposed SPR sensor can be applied to the near-mid infrared detection. Moreover, the maximum wavelength sensitivity of our proposed sensor can reach as high as 1.76×10^4 nm/refractive index unit (RIU) and the maximum wavelength interrogation resolution can be up to 5.68×10^{-6} RIU when the refractive index (RI) of analyte lies in (1.31, 1.36). Thanks to its excellent sensing performance, our proposed SPR sensor will have great potential applications for biological analytes detection, food safety control, bio-molecules detection and so on.

Keywords: surface plasmon resonance, holy fiber, fiber optics sensor

PACS: 07.07.Df, 42.81.Cn, 71.45.Gm **DOI:** 10.1088/1674-1056/ac43a5

1. Introduction

In recent years, surface plasmon resonance (SPR) sensors based on photonic crystal fiber (PCF) or holey fiber (HF) have attracted considerable interests due to their excellent sensing characteristics including high detection accuracy, level-free and real-time detection.[1–11] In PCF-based SPR sensing technology, the crucial factor is that the phase matching condition between the fiber core mode and the surface plasmon mode is fulfilled. However, the phase matching condition is always difficult to achieve since the difference of the refractive index between these two modes is usually large. Furthermore, the sensing property is highly dependent on the plasmon active metal materials since the optical properties of the metal materials have a large influence on the sensing performance, and in general, gold and silver are adopted.[12–17]

Nowadays, for the purpose of realizing the SPR effect and improving the sensing performance, a large number of PCF-SPR sensors with various novel designs have been investigated. Several PCF-based SPR sensors with typical structures are as follows. Rifat *et al.* designed a PCF-SPR sensor by employing a hexagonal-lattice structure.[18] Their simulation results showed that a maximum wavelength sensitivity of 3000 nm/refractive index unit (RIU) and a resolution of 2.4×10^{-5} RIU was achieved. In 2014, Otupiri *et al.* designed a PCF-SPR sensor with a slotted structure.[19] The resolution values of the *x*-polarized and *y*-polarized modes were up to 5×10^{-5} RIU and 6×10^{-5} RIU, respectively. Moreover, the amplitude sensitivities of these two polarized modes can be as high as 3×10^{-5} RIU and 4×10^{-5} RIU, respectively. In 2015, Rifat *et al.* designed a new type of PCF-SPR sensor by keeping the metallic film outside of the sensor structure.[20] The refractive index resolution of the sensor can reach to 2.5×10^{-5} RIU. In 2016, Huang designed a PCF-SPR sensor by using a D-shaped fiber structure.[21] The results showed that a high sensitivity of 6000 nm/RIU was realized through optimizing the sensor design. In 2017, Liu *et al.* designed a PCF-SPR sensor with two open-ring channels.[22] The resonance wavelength of the sensor lied in (2.55, 2.9) μm. The sensor maximum resolution and average wavelength sensitivity were 7.69×10^{-6} RIU and 5500 nm/RIU, respectively. In 2018, Tong *et al.* proposed a PCF-SPR sensor with muti-core design.[23] An average wavelength sensitivity of 3435 nm/RIU with a resolution of 2.91×10^{-6} RIU was achieved. In 2020, Wang *et al.* designed a PCF-SPR sensor with dual fiber structure.[24] The maximum spectral sensitivity and index resolution were as high as 17500 nm/RIU and 5.71×10^{-6} RIU correspondingly. However, in order to induce the efficient SPR effect, most of PCF-based SPR sensors are coated with gold or silver, which have several obvious limitations. On the one hand, the resonance bandwidth of these sensors coated with gold is always so broad that decreases the sensing performance because gold has a large absorption coefficient. Meanwhile, chemical properties of silver is unstable and is easily oxidized, which also destroys the detection accuracy.

In this paper, with the aim of overcoming the above limitations, a new type of SPR sensor based on circle lattice HF coated with indium tin oxide (ITO) is designed. By using of the full-vector finite element method, the sensing characteristics of our proposed sensor including wavelength sensitivity,

†Corresponding author. E-mail: Tianye_huang@163.com
© 2022 Chinese Physical Society and IOP Publishing Ltd

wavelength interrogation resolution, and amplitude sensitivity are numerically investigated carefully. The results show that the SPR effect can be efficiently enhanced by using a groove design, and the maximum wavelength interrogation sensitivity can reach to 1.76×10^4 nm/RIU.

2. Fiber design and theory

The structure diagram of our proposed HF-based SPR sensor is given in Fig. 1. The proposed sensor design includes two layers of air holes arranged in a circular lattice and a groove. For the purpose of enhancing the interaction between the core-guided mode and the SPP mode, there is a layer of ITO film located at the bottom of the groove. The main parameters of our proposed sensor are inner air hole diameter d_1, outer air hole diameter d_2, the pitch in the inner ring R_1, the pitch in the outer ring R_2, the spacing between the bottom of the groove and the central of the HF h, the width of the groove w, and the thickness of the ITO layer t. The refractive index (RI) of analyte is n_a. As the host material, the chromatic dispersion of silica is obtained by using the Sellmeier equation.[25] The permittivity of ITO is calculated by employing the Drude model[21]

$$\varepsilon = \varepsilon_\infty - \omega_p^2/\left(\omega^2 + \mathrm{i}\omega\Gamma\right), \tag{1}$$

$$\omega_p^2 = ne^2/(\varepsilon_\infty m^*), \tag{2}$$

where ε is the permittivity of ITO, $\varepsilon_\infty = 3.9$ is the high frequency permittivity, ω is the angular frequency, ω_p is the plasma frequency, $\Gamma = 1.8\times10^{14}$ rad/s is the electron scattering rate, $m^* = 0.35m_0$, $m_0 = 9.1\times10^{-31}$ kg is the rest mass of electrons, $n = 1.8\times10^{21}$ cm^{-3} is the carrier concentration of ITO, and e is the electron charge. Note that our proposed HF can be drawn by using the stack-and-draw technology while the groove structure can be achieved by using the focused ion-beam milling technology. The ITO layer can be deposited by employing the high-pressure chemical vapor deposition method.

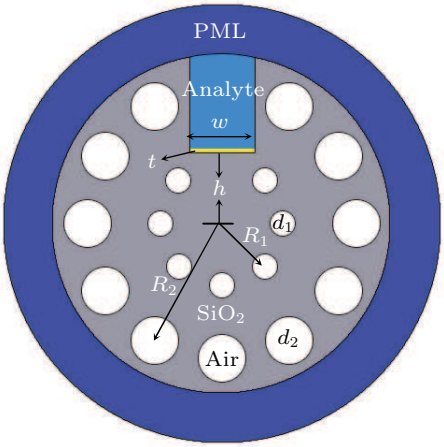


Fig. 1. The cross-structure of the proposed HF-based SPR sensor.

With the aim of investigating the sensing performance precisely, the sensor loss CL, wavelength sensitivity S_λ, detectable index resolution R and amplitude sensitivity S_a are calculated by adopting the following formulas:[21]

$$\mathrm{CL}\,(\mathrm{dB/cm}) = 8.686\times(2\pi/\lambda)\,\mathrm{Im}\,(n_{\mathrm{eff}})\times10^4, \tag{3}$$

$$S_\lambda\,(\mathrm{nm/RIU}) = \Delta\lambda_{\mathrm{peak}}\,(n_a)/\Delta n_a, \tag{4}$$

$$R\,(\mathrm{RIU}) = \Delta n_a\Delta\lambda_{\mathrm{min}}/\Delta\lambda_{\mathrm{peak}}, \tag{5}$$

$$S_a = -\left(\Delta\mathrm{CL}/\Delta n_a\right)/\mathrm{CL}_{\mathrm{initial}}, \tag{6}$$

where λ and $\mathrm{Im}\,(n_{\mathrm{eff}})$ are the wavelength and the imaginary part of the n_{eff}, correspondingly. $\Delta\lambda_{\mathrm{peak}}$ stands for the resonance wavelength variation. Δn_a denotes the RI changes. $\Delta\lambda_{\mathrm{min}}$ is the wavelength resolution of the instrument. ΔCL is the sensor loss changes while $\mathrm{CL}_{\mathrm{initial}}$ is the sensor loss at initial state.

3. Simulation results and discussion

For the purpose of calculating the electric field distribution and its modal effective index, we use a full-vector finite element method with the PML boundary conditions to solve Maxwell equations on the fiber structure and output the complex eigenvalues, and then the complex modal effective index can be obtained. The real part of the complex modal effective index ($\mathrm{Re}(n_{\mathrm{eff}})$) represents the modal dispersion property while the imaginary part of the complex modal effective index stands for the modal loss. Note that there are 118715 degrees of freedom over the whole holey fiber cross-section. Furthermore, the triangular and edge elements are 16934 and 1281, respectively. Firstly, we study the resonance properties of the sensor with parameters $d_1 = 1$ μm, $d_2 = 2$ μm, $R_1 = 2.5$ μm, $R_2 = 5.5$ μm, $w = 2.6$ μm, $h = 2.86$ μm, $t = 70$ nm, $n_a = 1.34$, and the simulation results indicate that only y-polarized fundamental mode can effectively interact with the surface plasmon polaritons (SPP) mode. Hence, the coupling properties between these two modes are investigated in this work. Figure 2 gives the modal profiles at different wavelength and dispersion properties of our proposed sensor. It is apparent from this figure that the real part of the refractive index of the y-polarized mode ($\mathrm{Re}(n_y)$) is much smaller than that of the SPP mode ($\mathrm{Re}(n_{\mathrm{spp}})$) in the short wavelength region. However, if the incident light wavelength increases to 1.555 μm, we can find that $\mathrm{Re}(n_y) = \mathrm{Re}(n_{\mathrm{spp}})$ since the SPR effect can modulate the phase of the electromagnetic wave. It means the phase-matching condition of the sensor is met. This resonance phenomenon can also be proved by the loss curve of the y-polarized mode, which exists a sharp loss peak at 1.555 μm. Moreover, the coupling property of the sensor can be studied from the mode distributions of the y-polarized fundamental and SPP modes, which are inserted in Fig. 2. Such as when $\lambda = 1.47$ μm, these two modes can not interact with each other because the

phase-matching condition is not met. But at 1.555 μm, the mode energy of the *y*-polarized mode is largely transferred into the SPP mode. Further increasing the light wavelength to 1.62 μm, these two modes become decoupled again since the coupling condition is destroyed.

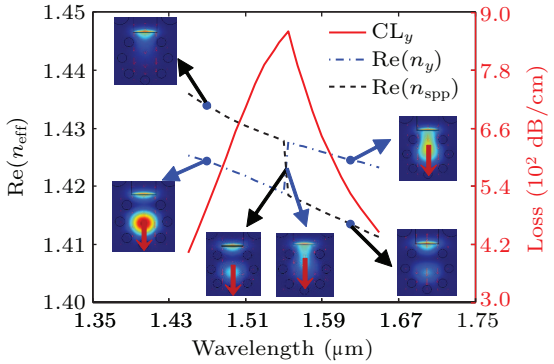


Fig. 2. The real parts of the effective indices and loss with $n_a = 1.34$. Insets are the electronic field profiles of two resonance modes.

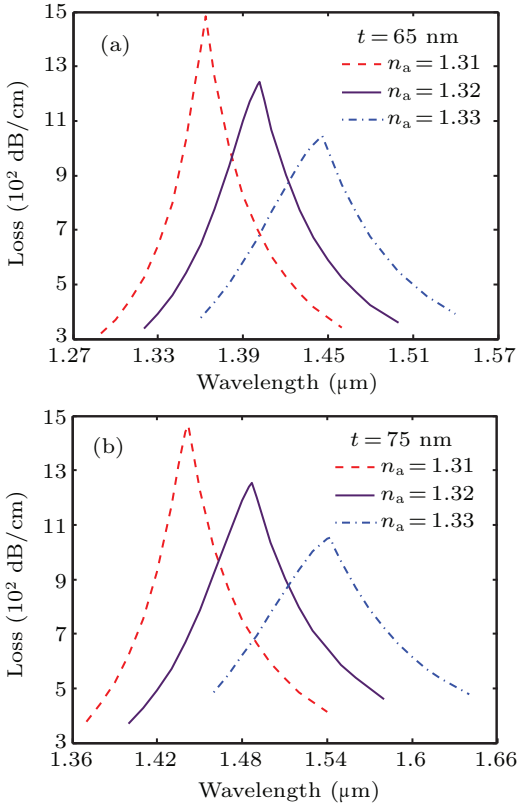


Fig. 3. Loss of the *y*-polarized fundamental mode by changing n_a from 1.31 to 1.33 when $t = 65$ nm and 75 nm.

Secondly, the effect of t on the sensing property with parameters $d_1 = 1$ μm, $d_2 = 2$ μm, $R_1 = 2.5$ μm, $R_2 = 5.5$ μm, $w = 2.6$ μm, and $h = 2.86$ μm is investigated. According to Fig. 3(a), it indicates that the resonance wavelength shifts to the longer wavelength by increasing n_a from 1.31 to 1.33 when $t = 65$ nm. For instance, the resonance wavelength is 1.364 μm at $n_a = 1.31$ while the resonance wavelength moves to 1.442 μm at $n_a = 1.33$. This is because Re(n_{spp}) increases with the increment of n_a while Re(n_y) almost keeps unchanged. Thus the phase matching point moves to the longer wavelength region. On the contrary, the peak loss decreases with increasing n_a from 1.31 to 1.33 when t is equal to 65 nm. The reason is that the interaction strength between the *y*-polarized fundamental mode and SPP mode decreases with the increment of n_a, and then less mode energy of the *y*-polarized mode is coupled into the SPP mode. Figure 3(b) gives the resonance property of our proposed sensor at $t = 75$ nm when n_a increases from 1.31 to 1.33. One can learn that the resonance and loss properties at $t = 75$ nm is similar to that of at $t = 65$ nm. However, compared Figs. 3(a) with 3(b), it can be found that the resonance wavelength at the same n_a shifts to the longer wavelength if t changes from 65 nm to 75 nm. According to Eq. (4), the wavelength sensitivities of 3800 nm/RIU and 4400 nm/RIU at $t = 65$ nm are obtained when n_a changes from 1.31–1.32 and 1.32–1.33, respectively. But if t increases to 75 nm, the wavelength sensitivities of the sensor increases to 4500 nm/RIU and 5500 nm/RIU when n_a changes from 1.31–1.32 and 1.32–1.33, respectively.

Besides wavelength interrogation sensitivity, amplitude sensitivity is another important factor to evaluate its sensing quality. Therefore, we study the influence of t on the amplitude sensitivity according to Eq. (6), and the numerical results are given in Fig. 4. Note that the sensor parameters are set to $d_1 = 1$ μm, $d_2 = 2$ μm, $R_1 = 2.5$ μm, $R_2 = 5.5$ μm, $w = 2.6$ μm and $h = 2.86$ μm. It is apparent from this figure that the value of the amplitude sensitivity is almost unchanged if t varies from 65 nm to 75 nm. For example, the maximum amplitude sensitivity is 83.29 RIU^{-1} at $t = 65$ nm while the maximum amplitude sensitivity is 82.39 RIU^{-1} at $t = 75$ nm. This is because if t varies from 65 nm to 75 nm, the coupling efficiency between these two modes is almost unchanged except that the coupling wavelength shifts to the longer wavelength, which is proved by Fig. 3. Moreover, the amplitude sensitivity curves move to the longer wavelength when the thickness of ITO film increases from 65 nm to 75 nm. Similar phenomena can be found in Refs. [26,27].

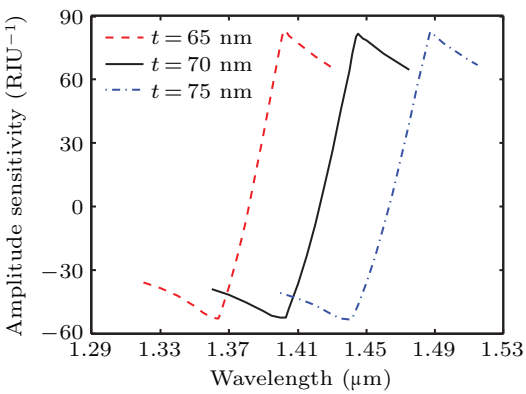


Fig. 4. Influence of the thickness of ITO film on the amplitude sensitivity with n_a varying from 1.31 to 1.32.

Table 1. Comparison of the sensing quality within n_a range from 1.31 to 1.36 when $t = 65$ nm, 70 nm and 75 nm, respectively.

	Peak wavelength (nm)			Peak loss (dB/cm)			Wavelength sensitivities (nm/RIU)			Maximum amplitude sensitivities (RIU^{-1})			Wavelength for the maximum amplitude sensitivity (nm)		
n_a \ t	65 nm	70 nm	75 nm	65 nm	70 nm	75 nm	65 nm	70 nm	75 nm	65 nm	70 nm	75 nm	65 nm	70 nm	75 nm
1.31	1364	1403	1442	1485	1447	1467	3800	4100	4500	83.29	82.78	82.39	1402	1445	1487
1.32	1402	1444	1487	1242	1229	1254	4400	5000	5500	69.09	67.47	66.78	1447	1494	1542
1.33	1446	1494	1542	1044	1036	1054	5400	6100	6800	58.28	56.02	53.97	1501	1555	1611
1.34	1500	1555	1610	866.3	860.2	879	6900	8000	9600	48.7	45.12	41.87	1570	1636	1706
1.35	1569	1635	1706	701.2	696.3	700.3	9800	12600	17600	38.24	32.78	25.19	1668	1761	1882
1.36	1667	1761	1882	542.5	524.7	517.3									

Table 2. Influence of h on the sensing quality when n_a varies from 1.31 to 1.36.

	Peak wavelength (nm)			Peak loss (dB/cm)			Wavelength sensitivities (nm/RIU)			Maximum amplitude sensitivities (RIU^{-1})			Wavelength for the maximum amplitude sensitivity (nm)		
n_a \ h	2.76 μm	2.86 μm	2.96 μm	2.76 μm	2.86 μm	2.96 μm	2.76 μm	2.86 μm	2.96 μm	2.76 μm	2.86 μm	2.96 μm	2.76 μm	2.86 μm	2.96 μm
1.31	1396	1403	1410	1522	1447	1389	4000	4100	4300	80.28	81.48	82.55	1437	1445	1453
1.32	1436	1444	1453	1290	1229	1179	4800	5000	5000	66.48	67.47	67.94	1485	1494	1504
1.33	1484	1494	1503	1086	1036	995.3	6000	6100	6400	55.32	56.02	56.25	1544	1555	1567
1.34	1544	1555	1567	898.2	860.2	827.2	7700	8000	8300	44.98	45.12	45.1	1621	1636	1651
1.35	1621	1635	1650	724.9	696.3	672.1	11900	12600	13300	32.98	32.78	32.27	1740	1761	1784
1.36	1740	1761	1783	546.4	524.7	506.6									

For the purpose of further investigating the sensing property of our proposed sensor, Table 1 gives the summary of several performance indexes within n_a range from 1.31 to 1.36 when $t = 65$ nm, 70 nm, and 75 nm, respectively. One can find from this Table that t has large influence on the peak wavelength, wavelength sensitivities and wavelength for the maximum amplitude sensitivity, but has small influence on the peak loss and maximum amplitude sensitivities. The resonance wavelength and the wavelength sensitivity of the designed sensor increase with increasing t from 65 nm to 75 nm when n_a lies in (1.31, 1.36). Such as when n_a is equal to 1.35, the peak wavelength and the wavelength sensitivity at $t = 65$ nm are 1.569 μm and 9800 nm/RIU while the peak wavelength and the wavelength sensitivity at $t = 75$ nm are up to 1.706 μm and 17600 nm/RIU, respectively. By using Eq. (5), we can obtain that the detectable index resolution can reach up to 5.68×10^{-6} RIU if the wavelength resolution of the instrument is 0.1 nm. Moreover, the changing trend of the wavelength for the maximum amplitude sensitivity is the same as that of the peak wavelength. The main reason is that the maximum amplitude sensitivity is proportional to the maximum ΔCL, which always happens nearby to the resonance wavelength. Benefiting from its excellent sensing property, our designed sensor should be very suitable for chemical and biological sensing applications. Note that the other parameters are set to $d_1 = 1$ μm, $d_2 = 2$ μm, $R_1 = 2.5$ μm, $R_2 = 5.5$ μm, $w = 2.6$ μm, and $h = 2.86$ μm.

Finally, we study the effect of h on the sensing performance with parameters $d_1 = 1$ μm, $d_2 = 2$ μm, $R_1 = 2.5$ μm, $R_2 = 5.5$ μm, $w = 2.6$ μm, and $t = 70$ μm when n_a varies from 1.31 to 1.36, and the simulation results are given in Table 2. According to this Table, we can learn that the peak loss decreases with increasing h from 2.76 μm to 2.96 μm when n_a keeps unchanged. The reason is that the interaction strength between these two modes becomes weaker if h changes from 2.76 μm to 2.96 μm. However, other performance parameters increase with the increment of h, especially the wavelength sensitivity. For example, the wavelength sensitivity increases from 11900 nm/RIU to 13300 nm/RIU with the increment of h from 2.76 μm to 2.96 μm when n_a changes from 1.35 to 1.36.

Table 3. Comparison of other PCF-SPR sensor sensitivity.

Authors	RI range (RIU)	Wavelength sensitivities (nm/RIU)	Reference
Rifat *et al.*	1.33–1.40	3000	[18]
Dash *et al.*	1.33–1.35	2000	[28]
Chen *et al.*	1.20–1.29	11055	[29]
Zhang *et al.*	1.31–1.37	11750	[30]
Wu *et al.*	1.37–1.40	4240	[31]
Abdullah *et al.*	1.33–1.40	48269.5	[32]
Bing *et al.*	1.33–1.44	11600	[33]
This work	1.31–1.36	17600	N/A

Table 3 gives a comparison of other PCF-SPR sensor sensitivity. Commonly, high sensitivity and high-accuracy detection makes our proposed sensor much more competitive than these traditional PCF-based SPR sensors.[18,28] Compared to these grooved PCF-based SPR sensors coated with gold or silver film,[29–31] the cost of our proposed HF-based SPR sensor coated with ITO is much lower. Furthermore, although other designs including inner-coated PCF-based SPR sensors have high sensitivity,[32,33] our proposed open-groove structure has the obvious advantages that an open-groove design is easier to fabricate and has an open sensing channel, which makes it very suitable for the real-time sensing.

4. Conclusion

In this paper, a new type of SPR sensor based on circular-lattice HF with an open sensing channel is proposed to achieve high sensitive sensing. The coupling resonance properties and sensing performance of our designed sensor are studied carefully. The research findings indicate that only the *y*-polarized fundamental mode can effectively interact with the SPP mode, which can efficiently eliminate the crossing interference between two fundamental polarized core modes. Furthermore, the maximum wavelength sensitivity and the detectable index resolution can reach as high as 17600 nm/RIU and 5.68×10^{-6} RIU, respectively. Benefiting from its excellent sensing characteristics, our proposed HF-based SPR sensor is of great potential for chemical and biological sensing applications.

Acknowledgements

Project supported by the National Natural Science Foundation of China (Grant No. 61765003) and the Scientific Research Foundation for the Wuyi University (Grant No. YJ202104).

References

[1] Yang Z, Xia L, Li C, Chen X and Liu D 2019 *Opt. Commun.* **430** 195
[2] Sharma A K, Kaur B and Marques C 2018 *Optik* **218** 164891
[3] Luan N N, Zhao L, Lian Y D and Lou S Q 2018 *IEEE Photonics J.* **10** 6803707
[4] Liu C, Su W, Wang F, Li X, Liu Q, Mu H, Sun T and Chu P K 2018 *IEEE Photo. Technol. Lett.* **30** 1471
[5] Ding Z P, Liao J F and Zeng Z K 2021 *Acta Phys. Sin.* **70** 074207 (in Chinese)
[6] Haque E, Hossain M A, Ahmed F and Namihira Y 2018 *IEEE Sens. J.* **18** 8278
[7] Liu J, Liang H Q, Liu B, He X D and Chen Z P 2019 *Opt. Fiber Technol.* **48** 248
[8] Pander A K, Sharma A K and Marques C 2020 *Materials* **13** 1623
[9] Sharma A K, Pandey A K and Kaur B 2018 *Opt. Fiber Technol.* **43** 20
[10] Zhao Y, Lei M, Liu S and Zhao Q 2018 *Sens. Actuators B Chem.* **261** 226
[11] Rahman Md M, Molla Md A, Paul A K, Based Md A, Rana Md M and Anower M S 2020 *Results Phys.* **18** 103313
[12] Han H, Hou D, Zhao L, Luan N, Song L, Liu Z, Lian Y, Liu J and Hu Y 2020 *Sensor* **20** 1009
[13] Li T, Zhu L, Yang X, Lou X and Yu L 2020 *Sensor* **20** 741
[14] Fan Z 2019 *Opt. Fiber Technol.* **50** 194
[15] Azzam S I, Hameed M F O, Shehata R E A, Heikal A and Obayya S 2016 *Opt. Quantum. Electron.* **48** 1
[16] Rifat A A, Ahmed R, Mahdiraji G A and Adikan F R M 2017 *IEEE Sens. J.* **17** 2776
[17] Dash J N and Jha R 2015 *Plasmonics* **10** 1123
[18] Rifat A A, Mahdiraji G A, Chow D M, Shee Y G, Ahmed R and Adikan F R M 2015 *Sensor* **15** 11499
[19] Otupiri R, Akowuah E, Haxha S, Ademgil H, AbdelMalek F and Aggoun A 2014 *IEEE Photonics J.* **6** 6801711
[20] Rifat A A, Mahdiraji G A, Sua Y M, Shee Y G, Ahmed R, Chow D M and Adikan F R M 2015 *IEEE Photo. Technol. Lett.* **27** 1628
[21] Huang T 2017 *Plasmonics* **12** 583
[22] Liu C, Yang L, Lu X, Liu Q, Wang F, Lv J, Sun T, Mu H and Chu P K 2017 *Opt. Express* **25** 14227
[23] Tong K, Wang F, Wang M, Dang P and Wang Y 2018 *Opt. Fiber Technol.* **46** 306
[24] Wang J, Liu C, Wang F, Su W, Yang L, J Lv, Fu G, Li X, Liu Q, Sun T and Chu P K 2020 *Results Phys.* **18** 103240
[25] Ghosh G, Endo M and Iwasaki T 1994 *J. Lightwave Technol.* **12** 1338
[26] Liao J, Ding Z, Xie Y, Wang X, Zeng Z and Huang T 2020 *Opt. Fiber Technol.* **60** 102316
[27] Chakma S, Khalek M A, Paul B K, Ahmed K, Hasan M R and Bahar A N 2018 *Sens. Bio-Sens. Res.* **18** 7
[28] Dash J N and Jha R 2014 *IEEE Photo. Technol. Lett.* **26** 595
[29] Chen X, Xia L and Li C 2018 *IEEE Photonics J.* **10** 6800709
[30] Zhang S, Li J, Li S, Liu Q, Wu J and Guo Y 2018 *J. Phys. D: Appl. Phys.* **51** 305104
[31] Wu M, Liu X Y, Zhou G Y, Xia C M, Li B Y and Hou Z Y 2019 *Chin. Phys. B* **28** 124202
[32] Abdullah H, Ahmed K and Mitu S A 2020 *Results Phys.* **17** 103151
[33] Bing P, Sui J, Wu G, Guo X, Li Z, Tan L and Yao J 2020 *Plasmonics* **15** 1071